The Effects of Turbulence on Three-Dimensional Magnetic Reconnection at the Magnetopause

L. Price, M. Swisdak, J. F. Drake, and J. Dahlin
IREAP, University of Maryland, College Park MD 20742-3511, USA

P. A. Cassak
Department of Physics, West Virginia University, Morgantown, West Virginia 26506, USA

R. E. Ergun
Department of Astrophysical and Planetary Sciences, University of Colorado, Boulder, Colorado, 80303, USA

arXiv:1604.08172v2 [physics.space-ph] 7 Jun 2016

Two- and three-dimensional particle-in-cell simulations of a recent encounter of the Magnetospheric Multiscale Mission (MMS) with an electron diffusion region at the magnetopause are presented. While the two-dimensional simulation is laminar, turbulence develops at both the x-line and along the magnetic separatrices in the three-dimensional simulation. The turbulence is strong enough to make the magnetic field around the reconnection island chaotic and produces both anomalous resistivity and anomalous viscosity. Each contribute significantly to breaking the frozen-in condition in the electron diffusion region. A surprise is that the crescent-shaped features in velocity space seen both in MMS observations and in two-dimensional simulations survive, even in the turbulent environment of the three-dimensional system. This suggests that MMS's measurements of crescent distributions do not exclude the possibility that turbulence plays an important role in magnetopause reconnection.

I. INTRODUCTION

Magnetic reconnection facilitates the conversion of magnetic energy to high-speed plasma flows and thermal energy. This energy release requires a change in the topology of the field, which occurs at magnetic x-lines. Electron diffusion regions (EDRs), which surround x-lines, are small, with characteristic thicknesses given by the electron skin depth $d_e = c/\omega_{pe}$, where ω_{pe} is the electron plasma frequency. The detection of EDRs is the prime motivation for the Magnetospheric Multiscale Mission (MMS).

The first stage of MMS has focused on the magnetopause, where the differences between magnetospheric and magnetosheath plasma produce asymmetric reconnection. Some distinctive features of electron distribution functions associated with the EDRs of asymmetric reconnection have been recently identified [1, 2, 11, 20]. In particular, the strong asymmetry in density across the magnetopause causes a large component of the electric field perpendicular to the current sheet, E_N, to form which, in turn, prevents the high-density magnetosheath ions from crossing the magnetopause. (In the LMN coordinate system L is in the direction of the reconnecting magnetic field, N parallels the inflow direction and M is perpendicular to L and N in the out-of-plane direction.) This E_N accelerates the unmagnetized electrons near the magnetic null toward the magnetosphere, where they are turned by B_L into the M direction. The result is cusp-like electron orbits on the earthward side of the x-line and along the separatrices on the earthward edges of the reconnection exhaust. The consequence is crescent-shaped velocity-space distributions which were first noted in numerical simulations [11]. Parallel electric fields downstream from the x-line also produce crescents along the outflow direction and were first identified in the MMS data [2].

Most simulations of reconnection treat a reduced geometry in which variations in the out-of-plane direction are ignored. This treatment eliminates fluctuations with wavevectors in the invariant direction and hence greatly inhibits the development of turbulence, which is typically driven by the strong out-of-plane current in the diffusion region. Reconnection in this limit is essentially laminar, although current-driven instabilities along the separatrices can produce intense parallel electric fields [4, 13]. Since crescents are only observed in regions of large E_N where the electron out-of-plane current J_M is also large, the turbulence that is expected to develop within these current layers might plausibly scatter the electron orbits and destroy the crescents. Thus, the fact that crescent-shaped features are observed in MMS distribution functions suggests that actual magnetopause reconnection is laminar. The sensitivity of the electron crescents to the development of turbulence remains an open issue.

A primary goal of MMS is to determine what breaks the frozen-in condition during reconnection or, equivalently, what terms in Ohm's law balance the out-of-plane reconnection electric field E_M in the EDR. During asymmetric reconnection, the stagnation point of the normal electron flow v_{eN} is displaced toward the magnetosphere side of the x-point [3]. In two-dimensional simulations the M component of the divergence of the pressure tensor balances E_M at the stagnation point, but E_M at the x-point can be balanced by various terms (depending on the configuration), including the electron inertia

$m_e v_{eN} \partial v_{eM}/\partial N$ [11]. An important question is whether the turbulence that develops in the diffusion region alters these conclusions.

In this paper we present three-dimensional simulations of reconnection with initial conditions reflective of the MMS event described in [2]. Because of the extra freedom associated with dynamics in the dawn-dusk (M) direction, instabilities such as the lower-hybrid drift instability (LHDI) [16–19] or the electron Kelvin-Helmholtz instability [14] can develop. In contrast with the results of earlier simulations [16, 19], we find that for the parameters associated with the MMS event, which has a larger jump in plasma density than had been previously treated, the turbulence significantly deforms the current layers and produces variations in the electromagnetic fields sufficiently strong to affect the structure of the diffusion region: anomalous resistivity and anomalous viscosity both play a role in breaking the frozen-in condition. (Interestingly, high-frequency electric field fluctuations, amplitude $\gtrsim$ 20 mV/m, were seen in the EDR during the MMS crossing.) However, in spite of the presence of turbulence in the simulations, crescents are still present in the electron distribution functions within the strong current layers on the magnetospheric edge of the diffusion region and separatrices. Thus, the role of turbulence in balancing Ohm's law remains an open issue in the MMS observations.

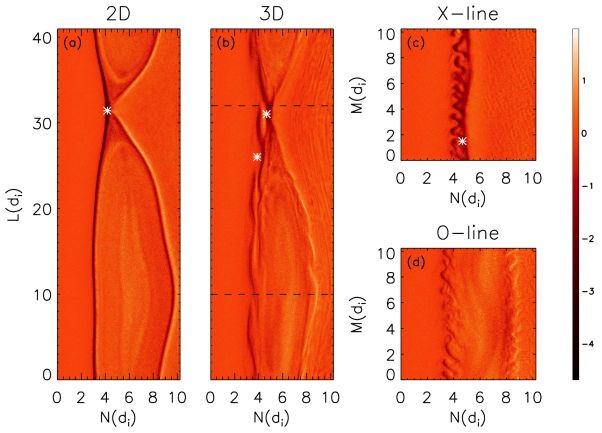

FIG. 1. Snapshots of J_{eM}, the dawn-dusk electron current density. Panel (a): The $L-N$ plane from the two-dimensional simulation at $t = 40$. Panel (b): The $L-N$ plane from the three-dimensional simulation when roughly the same amount of flux has reconnected ($t = 30$). The two dashed lines denote the cuts shown in subsequent panels. Panel (c): The $M-N$ plane from a cut through the x-line, the upper line in panel (b). Panel (d): The $M-N$ plane from a cut through the island, the lower line in panel (b). In each panel the colors are separately normalized; the bar at the right shows the relative variation. The stars indicate the locations of the distribution functions presented in Figure 4.

II. SIMULATIONS

We use the particle-in-cell code `p3d` [23]. The magnetic field strength B_0 and density n_0 define the Alfvén speed $v_{A0} = \sqrt{B_0^2/4\pi m_i n_0}$, with lengths normalized to the ion inertial length $d_i = c/\omega_{pi}$, where ω_{pi} is the ion plasma frequency, and times to the ion cyclotron time Ω_{i0}^{-1}. Electric fields and temperatures are normalized to $v_{A0}B_0/c$ and $m_i v_{A0}^2$, respectively.

The initial conditions for the simulations closely mimic those observed by MMS during the diffusion region encounter discussed in [2]. The particle density n, reconnecting field component B_L, and ion temperature T_i vary as a function of N with hyperbolic tangent profiles of width 1. The asymptotic values of n, B_L, and T_i are 1.0, 1.0 and 1.37 in the magnetosheath and 0.06, 1.70, and 7.73 in the magnetosphere. The guide field $B_M = 0.099$ is initially uniform. Pressure balance determines the electron temperature T_e, subject to the constraint that its asymptotic magnetosheath value is 0.12. (The asymptotic value of T_e in the magnetosphere is thus 1.28.) Although the system is in force balance, the initial conditions are not an exact Vlasov equilibrium. Following initialization the system adjusts and reaches the steady-state configuration analyzed here.

We performed both two-dimensional and three-dimensional simulations with these parameters. For the two-dimensional simulation the domain had dimensions $(L_L, L_N) = (40.96, 20.48)$ and employed the same plasma parameters as that discussed in [2]. The three-dimensional simulation extended the M direction: $(L_L, L_M, L_N) = (40.96, 10.24, 20.48)$. The ion-to-electron mass ratio was set to 100, which is sufficient to separate the electron and ion scales. The spatial grid has a resolution $\Delta = 0.02$ while the smallest physical scale is the Debye length in the magnetosheath, ≈ 0.03. As in [2] we used 500 particles per cell per species when $n = 1.0$ for the two-dimensional simulation. Due to computational constraints, the three-dimensional simulation uses 50 particles per cell, which implies ≈ 3 particles per cell in the low-density magnetosphere. To mitigate the resulting noise, our analysis of this case employs averages over multiple cells.

The velocity of light is $c = 15$ so that $\omega_{pe}/\Omega_{ce} = 1.5$ in the asymptotic magnetosheath and 0.3 in the asymptotic magnetosphere; the observed ratios are larger (≈ 35 and 6, respectively). As a result, the Debye length in the simulation is not as small as at the magnetopause and might artificially suppress very short wavelength electrostatic instabilities [12]. Unlike some earlier simulations of [19] we do not force the rate of reconnection with an external boundary condition; instead, the boundary conditions are periodic in all directions. Our initial profiles also differ from those earlier simulations (the density jump across the magnetopause being 16 rather than 10) since they have been chosen to match the event explored by MMS.

Figure 1 displays images of J_{eM}, the dawn-dusk electron current density. Panels (a) and (b) show the $L-N$

plane for the two-dimensional and three-dimensional simulations after reconnection of roughly the same amount of magnetic flux. In both, the magnetosphere (strong field, low density) is to the left and the magnetosheath (weak field, high density) is to the right. As is typical in asymmetric configurations, the reconnection of equal amounts of flux from the two sides means the islands bulge into the magnetosheath. While the two-dimensional simulation is laminar, turbulence develops in the three-dimensional case. This can be clearly seen in panels (c) and (d), which show J_{eM} in cuts through the $M-N$ plane of the simulation at the locations denoted by the dashed lines in panel (b). The current layers at both the x-line (panel c) and bordering the magnetic island (panel d) have become turbulent.

The free energy in the strong, spatially localized, out-of-plane electron flows are the likely drive for the instability. The wavelength is consistent with the lower-hybrid drift instability (LHDI) both near the x-line and on the separatrices during asymmetric reconnection. The energy source for the LHDI is the relative drift of the ions and electrons in the M direction and the wavevector satisfies the relation $\mathbf{k}\cdot\mathbf{B}=0$ so that $\mathbf{k}$ is along M at the x-line and the midplane of the island. Thus, the LHDI does not develop in the two-dimensional simulation. Within the current layer, the range of excited wavenumbers is relatively broad, $(m_e/m_i)^{0.25} \lesssim k\rho_e \lesssim 1$, where ρ_e is the thermal electron Larmor radius [7]. For the parameters of our simulations, this can be written as a condition on the wavelength: $0.5 \lesssim \lambda/d_i \lesssim 2$. The fluctuations in the simulation fall within this range. On the other hand, the strong, localized electron drift seen in Figure 1 differs from systems usually analyzed for the LHDI instability and the electron Kelvin-Helmholtz instability [14] is also a possible driver for the turbulence. Note that while the instability has reached the non-linear stage by the time shown in panels (c) and (d), the structure at earlier times (not shown) exhibits similar spatial scales. The presence of strong turbulence around the x-line differs from the results of earlier three-dimensional simulations, where strong turbulence was largely localized away from the x-line along the separatrices.

The flows driven by the instability are dominantly in the $M-N$ plane and twist the dominant magnetic field (L direction) so that it develops M and N components. We emphasize, however, that the development of B_M and B_N is a conversion from flow to magnetic energy rather than the reverse. Nevertheless, the result is a chaotic magnetic field. Figure 2 shows the intersections of field lines with the $M-N$ plane at the midplane of the magnetic island with J_{eM} in the background. Because of the periodic boundary conditions, each field line passes through the simulation multiple times, although each pass can also be considered a separate field line. On the left side, in the upstream magnetosphere, the field is laminar. A band of magnetic flux ropes borders this region, just to the left of the strongest turbulence which peaks at $N \approx 3.5$. These coherent structures bound the

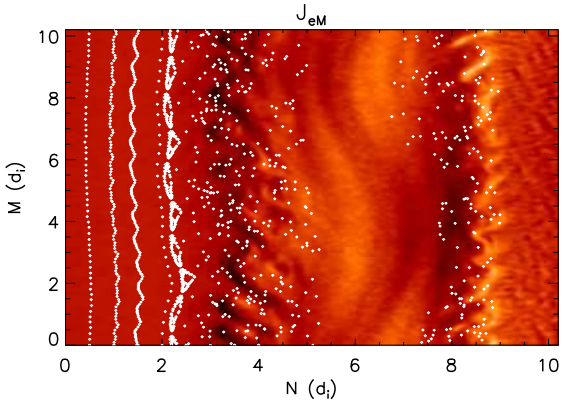

FIG. 2. Puncture plot showing the intersections of field lines with panel (d) of Figure 1. Each dot represents the intersection of a field line with the plane after tracing its trajectory through the simulation domain. The islands at $N \approx 2.5$ mark the transition from laminar to turbulent behavior.

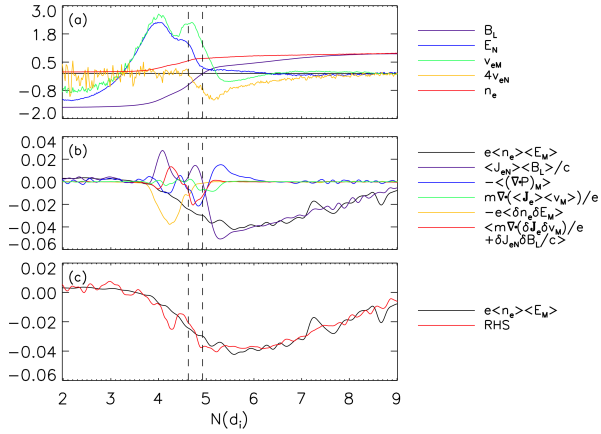

FIG. 3. Cuts in the N direction through the electron diffusion region for the three-dimensional simulation. Panel (a): The density n_e, reconnecting magnetic field B_L, the normal electric field E_N, and the electron flows v_{eN} and v_{eM} all averaged over M. Panel (b): The principal terms in Ohm's law from equation 3. (Additional small terms are included, as noted by the key, but produce minimal effects.) Panel (c): The sum of the left and right sides of equation 3. In each panel the vertical lines show the approximate positions of the stagnation point ($N \approx 4.5$) and x-point ($N \approx 4.9$).

chaotic field lines that fill the large-scale magnetic island. (The field lines within the island intersect the plane twice, once at $2.5 \lesssim N \lesssim 5$ and again at $7 \lesssim N \lesssim 8.5$.) The twisting of flux ropes by the vortical $M-N$ flows is similar to that inferred from MMS observations by [10].

The role of turbulence can be quantified by evaluating the terms of the generalized Ohm's law in a cut through the x-line. We begin with the momentum equation for the electron fluid

$$en\mathbf{E} = -mn\frac{d\mathbf{v}}{dt} - \boldsymbol{\nabla}\cdot\mathbb{P} - en(\mathbf{v}/c)\times\mathbf{B} \qquad (1)$$

where m, n, $\mathbf{v}$, and $\mathbb{P}$ are the electron mass, density, velocity, and pressure tensor (we only refer to electrons below and so have dropped the species subscripts). Taking the out-of-plane (M) component gives, after invoking symmetry with respect to the L coordinate near the x-line [11],

$$enE_M = -env_N B_L/c - \left(\frac{\partial P_{LM}}{\partial L} + \frac{\partial P_{NM}}{\partial N} + \frac{\partial P_{MM}}{\partial M}\right) - m\left(\frac{\partial}{\partial t}nv_M + \frac{\partial}{\partial N}nv_N v_M\right) \quad (2)$$

In the two-dimensional case $\partial P_{MM}/\partial M = 0$.

In Figure 3a we highlight the basics of asymmetric reconnection by plotting some of the key parameters on a cut along N through the x-line: n, B_L, E_N, v_M and v_N. The magnetosphere is on the left and the magnetosheath on the right. For asymmetric reconnection the stagnation point, where $v_N = 0$, lies on the magnetosphere side of the x-point, where $B_L = 0$ [3]. The vertical dashed lines in the figure indicate the approximate locations of these points. The high-speed electron flow v_M is dominantly driven by E_N and these two quantities track each other across the diffusion region. The qualitative behavior of cuts through the two-dimensional simulation (not shown) is similar to Figure 3a and consistent with the results of [11]. The electron inertia term balances E_M where $B_L = 0$ and the divergence of the pressure tensor balances E_M where $v_N = 0$.

To establish the role of turbulence in the three-dimensional simulation, we average over the M direction and decompose every quantity into a mean and fluctuating component, i.e., $n = \langle n\rangle + \delta n$. Note that products of quantities produce two terms, $\langle AB\rangle = \langle A\rangle\langle B\rangle + \langle \delta A \delta B\rangle$. Keeping the most significant terms in equation 2 gives

$$e\langle n\rangle\langle E_M\rangle = \langle J_N\rangle\langle B_L\rangle/c - \left[\frac{\partial}{\partial L}\langle P_{LM}\rangle + \frac{\partial}{\partial N}\langle P_{NM}\rangle\right] + \frac{m}{e}\left[\frac{\partial}{\partial L}\langle J_L\rangle\langle v_M\rangle + \frac{\partial}{\partial N}\langle J_N\rangle\langle v_M\rangle\right] - e\langle\delta n\delta E_M\rangle + \left\langle \delta J_N \delta B_L/c + \frac{m}{e}\frac{\partial}{\partial N}\delta J_N \delta v_M\right\rangle \quad (3)$$

In deriving equation 3, the weak time-dependence has been dropped since we are focusing on steady-state behavior. We have also discarded terms containing J_L and δJ_L that symmetry arguments suggest are small (and which we have confirmed are small in the simulation data).

The first three terms on the right-hand side involve only mean quantities and can be matched to terms in equation 2. They represent the usual contributions from the convective motion, pressure tensor, and inertial terms. The final two terms arise from the fluctuations and can be interpreted as contributions from an anomalous resistivity and an anomalous viscosity associated with the turbulent transport of the canonical momentum $mv_M - eA_M/c$ with $B_L = \partial A_M/\partial N$, where $\mathbf{A}$ is the vector potential [5].

Figure 3(b) displays the separate terms of equation 3 and Figure 3(c) shows the left side and the total of all of the terms on the right side. (While equation 3 includes only the most significant terms, all but the time-dependent term were kept for the figure.) The anomalous resistivity term $\langle\delta n\delta E_M\rangle$ is large around the stagnation point but diminishes near the x-point while the viscosity term is significant over a broad region between the two. Without the inclusion of these terms, the two curves in panel (c) would not match. Thus, turbulent effects are playing an essential role in balancing the reconnection electric field.

Recent investigations of particle distributions in two-dimensional asymmetric reconnection have revealed crescent-shaped features in the $v_M - v_N$ phase space of electrons. These are signatures of the cusp-like motion produced by the combination of E_N and a gradient in B_L [1, 2, 20]. If, in the electron current layers driven by E_N, the turbulence is sufficiently strong the fluctuating electric fields might scatter the electron orbits, preventing the formation of the crescent distributions. Of course, if the electrons were simply gyrating around the $\mathcal{O}(1)$ field, the turbulence would not strongly affect the orbits unless the turbulence frequency was comparable to Ω_{ce}. However, instead the orbits are cusp-like and unmagnetized close to the magnetic null where they are directly accelerated by E_N across B_L [1, 20]. The motion along N is then turned into the M direction by B_L to produce the electron drift v_{eM}. If the turbulence breaks up the current layer so that the components of E_M and E_N are comparable, the electrons will be directly accelerated in both the N and M directions, potentially disrupting the cusp-like motions.

However, Figure 4 suggests that the crescents survive even when the turbulence in the electron current layers is strong. Panel a displays data from a region upstream of the x-line on the magnetosphere side from the two-dimensional simulation. The crescent is clearly visible, consistent with earlier simulations [6, 11, 20] and the MMS data [2]. Data from the three-dimensional simulation, also taken from the magnetospheric side of the x-line, is shown in panels b and c. For panel b the distribution is taken over a limited range in the out-of-plane direction $1 \le M \le 1.25$ while panel c is taken over all M. The crescent is clearly present in panel b. In panel c, integration over the larger range in M samples many periods of the turbulence and smears out, but does not destroy, the crescent. Panel d shows a distribution taken near the separatrix but downstream from the x-line in the three-dimensional simulation. A crescent feature is still visible.

The crescents from the two-dimensional and three-dimensional simulations do exhibit some qualitative differences. The noisier distribution of panel a is a consequence of the smaller number of particles (and hence larger random noise) per velocity bin. Second, the two-

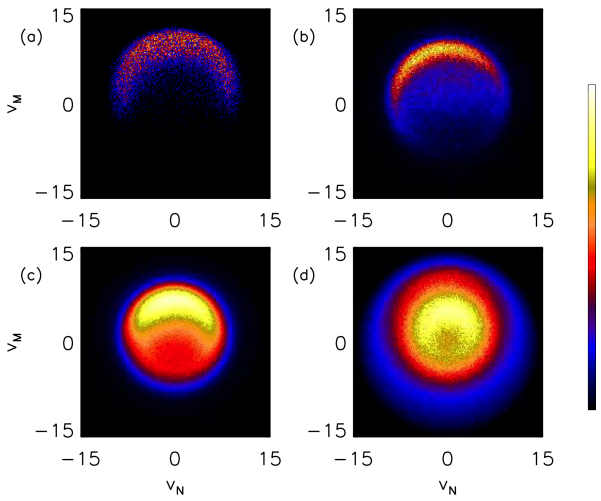

FIG. 4. $v_N - v_M$ electron distribution functions from the two-dimensional (panel a) and three-dimensional (panels b-d) simulations. The distributions were taken at the positions shown by the stars in Figure 1. Panels b and c were taken near the x-line. In panel b only a limited range in M was sampled, $1 \leq M \leq 1.25$; panels c and d sample the entire box, $0 \leq M \leq 10.24$. Panel d was taken near the separatrix, downstream from the x-line (see Figure 1). The number of particles in each velocity bin is plotted on a linear scale that is different for each panel, although the color bar shows the relative variation.

dimensional case shows a faster bulk flow in the M direction. This is because the electron current layer in the two-dimensional case remains highly localized in the N direction. In contrast, the turbulence in the three-dimensional run broadens the current layer. Since the integrated current across the layer must be the same in both cases, the broader layer from the three-dimensional run produces a smaller bulk velocity. On the other hand, the small counter-clockwise rotation observable in panel b is simply a consequence of the location at which the distribution is taken. Similar rotations can be seen in the two-dimensional simulation for distributions from nearby locations.

III. DISCUSSION

Reconnection in asymmetric configurations can be stabilized by the presence of diamagnetic drifts [15, 21, 22], with complete stabilization occurring when the difference in $\beta = 8\pi P/B^2$ between the asymptotic plasmas exceeds $\tan\theta/2$, where θ is the shear angle between the reconnecting fields. In the configuration considered here, $\Delta\beta \approx 2.5$ is relatively large but, because the guide field is small, $\theta \approx 170^\circ$ is also large. Hence reconnection is unaffected by diamagnetic drifts, which is in agreement with the reconnection rate of $\mathcal{O}(0.1)$ observed for the both the two-dimensional and three-dimensional simulations. As a separate effect, a finite guide field can affect the development of structures in the out-of-plane direction. Because $B_M/B_L \lesssim 0.1$ is small in this case, however, the oblique tearing mode and the development of flux ropes, as seen in [8], does not occur in our domain.

An important question is whether real mass-ratio simulations would yield results that differ significantly from the present simulations where $m_i/m_e = 100$. We suggest that the results should not be sensitive to the mass ratio. Even with real mass ratios the LHDI is strong in systems with scale lengths near the ion Larmor scale, which is characteristic of the boundary layers with strong E_N at the magnetopause. The suppression of LHDI by magnetic shear and finite β is weaker in asymmetric reconnection because the strongest density gradient and peak current J_{eM}, which drive the instability, are on the magnetosphere side of the x-line where β is smaller. The strongest turbulent drag (Figure 3(b)) is peaked near the stagnation point ($v_{eN} = 0$), well away from the magnetic null. The anomalous viscosity terms (Figure 3(b)) peak in the region between the magnetic null and the stagnation point where the gradients in v_{eM} are greatest and have scale lengths below d_i.

In a recent paper [10] report on MMS observations of very intense parallel electric fields found in small-scale structures along the magnetospheric separatrices during magnetopause reconnection. They associate these parallel electric fields with localized reconnection events in which the magnetic field is twisted by vortical plasma motions in the $M-N$ plane. The magnetic turbulence that develops along the separatrices of our three-dimensional simulations is reminiscent of these observations – the strong electron flows basically twist up the magnetic field. On the other hand, the parallel electric fields in our simulations are not as intense as in the MMS data (≈ 10 versus ≈ 100 mV/m) and are largest in the diffusion region rather than along the separatrices. Cuts of $E_\parallel$ in the $M-N$ plane through the x-line (not shown) reveal electron holes similar to those seen in earlier simulations with larger guide fields [9]. One possible explanation for this discrepancy may be the artificially low mass ratio. A realistic value could yield sharper gradients and more intense fields. It is also possible that in our simulations we are only exploring the early stages of the dynamics of these turbulent current layers. With larger simulations that could be evolved for longer times it is possible that the strong parallel currents that develop along the separatrices might form more intense localized parallel electric fields as seen in some earlier two-dimensional simulations [4, 13].

The role that turbulence might have in breaking the frozen-in condition has not yet been explored with the MMS data. On the other hand, short bursts of $E_M \sim 10$ mV/m were seen in the current layer where E_N is large [2]. Thus, the presence of turbulence seems likely but its consequences and the specific correlated averages that need to be carried out to evaluate the anomalous drag and viscosity coefficients in equation 3 have not been evaluated.

In conclusion, we find that the inclusion of the third dimension permits the development of strong turbulence, both at the x-line and along the separatrices. This turbulence makes significant contributions to the balance of Ohm's law but, perhaps surprisingly, does not disrupt the formation of crescent features in the velocity distribution functions. Hence, the existence of such crescents cannot serve as an indicator as to whether turbulence plays an important role at a reconnection x-line.

ACKNOWLEDGMENTS

This work was supported by NASA grants NNX14AC78G, NNX16AG76G, and NNX16AF75G and NSF grants PHY1500460, AGS-0953463, and AGS-1460037. The simulations were carried out at the National Energy Research Scientific Computing Center. The data used to perform the analysis and construct the figures for this paper are available upon request.

[1] Bessho, N., L.-J. Chen, and M. Hesse (2016), Electron distribution functions in the diffusion region of asymmetric magnetic reconnection, *Geophys. Res. Lett.*, *43*, 1828–1836, doi:10.1002/2016GL067886.

[2] Burch, J. L., et al. (2016), Electron-scale measurements of magnetic reconnection in space, *Science*, doi: 10.1126/science.aaf2939.

[3] Cassak, P. A., and M. A. Shay (2007), Scaling of asymmetric magnetic reconnection: General theory and collisional simulations, *Phys. Plasmas*, *14*, 102114, doi: 10.1063/1.2795630.

[4] Cattell, C., et al. (2005), Cluster observations of electron holes in association with magnetotail reconnection and comparison to simulations, *J. Geophys. Res.*, *110*, A01211, doi:10.1029/2004JA010519.

[5] Che, H., J. F. Drake, and M. Swisdak (2011), A current filamentation mechanism for breaking field magnetic field lines during reconnection, *Nature*, *474*, 184–187, doi: 10.1038/nature10091.

[6] Chen, L.-J., M. Hesse, S. Wang, N. Bessho, and W. Daughton (2016), Electron energization and structure of the diffusion region during asymmetric reconnection, *Geophys. Res. Lett.*, *43*, doi:10.1002/2016GL068243.

[7] Daughton, W. (2003), Electromagnetic properties of the lower-hybrid drift instability in a thin current sheet, *Phys. Plasmas*, *10*(3103), doi:10.1063/1.1594724.

[8] Daughton, W., V. Roytershteyn, H. Karimabadi, L. Yin, B. J. Albright, B. Bergen, and K. J. Bowers (2011), Role of electron physics in the development of turbulent magnetic reconnection in collisionless plasmas, *Nature Phys.*, *7*, 539–542, doi:10.1038/nphys1965.

[9] Drake, J. F., M. Swisdak, C. Cattell, M. A. Shay, B. N. Rogers, and A. Zeiler (2003), Formation of electron holes and particle energization during magnetic reconnection, *Science*, *299*(5608), 873–877, doi: 10.1126/science.1080333.

[10] Ergun, R. E., et al. (2016), MMS observations of parallel electric fields associated with magnetic reconnection, *Phys. Rev. Lett.*, accepted.

[11] Hesse, M., N. Aunai, D. Sibeck, and J. Birn (2014), On the electron diffusion region in planar, asymmetric systems, *Geophys. Res. Lett.*, *41*(24), doi: 10.1002/2014GL061586.

[12] Jara-Almonte, J., W. Daughton, and H. Ji (2014), Debye scale turbulence within the electron diffusion layer during magnetic reconnection, *Phys. Plasmas*, *21*, 032114, doi: 10.1063/1.4867868.

[13] Lapenta, G., S. Markidis, A. Divin, M. V. Goldman, and D. L. Newman (2011), Bipolar electric field signatures of reconnection separatrices for a hydrogen plasma at realistic guide fields, *Geophys. Res. Lett.*, *38*(17), doi: 10.1029/2011GL048572.

[14] Lee, S.-Y., E. Lee, K.-H. Kim, D.-H. Lee, J. Seon, and H. Jin (2015), Electron Debye scale Kelvin-Helmholtz instability: electrostatic particle-in-cell simulations, *Phys. Plasmas*, *22*(122113), doi:10.1063/1.4938201.

[15] Phan, T. D., G. Paschmann, J. T. Gosling, M. Øieroset, M. Fujimoto, J. F. Drake, and V. Angelopoulos (2013), The dependence of magnetic reconnection on plasma β and magnetic shear: Evidence from magnetopause observations, *Geophys. Res.. Lett.*, *40*, 11–16, doi: 10.1029/2012GL054528.

[16] Pritchett, P. L. (2013), The influence of intense electric fields on three-dimensional asymmetric magnetic reconnection, *Phys. Plasmas*, *20*, 061204, doi: 10.1063/1.4811123.

[17] Pritchett, P. L., and F. S. Mozer (2011), Rippling mode in the subsolar magnetopause current layer and its influence on three-dimensional magnetic reconnection, *J. Geophys. Res.*, *116*, A04215, doi:10.1029/2010JA016190.

[18] Pritchett, P. L., F. S. Mozer, and M. Wilber (2012), Intense perpendicular electric fields associated with three-dimensional magnetic reconnection at the subsolar magnetopause, *J. Geophys. Res.*, *117*, A06212, doi: 10.1029/2012JA017533.

[19] Roytershteyn, V., W. Daughton, H. Karimabadi, and F. S. Mozer (2012), Influence of the lower-hybrid drift instability on magnetic reconnection in asymmetric configurations, *Phys. Rev. Lett.*, *108*, 185001, doi: 10.1103/PhysRevLett.108.185001.

[20] Shay, M. A., T. D. Phan, C. C. Haggerty, M. Fujimoto, J. F. Drake, K. Malakit, P. A. Cassak, and M. Swisdak (2016), Kinetic signatures of the region surrounding the x-line in asymmetric (magnetopause) reconnection, *Geophys. Res. Lett.*, *43*, doi:10.1002/2016GL069034.

[21] Swisdak, M., B. N. Rogers, J. F. Drake, and M. A. Shay (2003), Diamagnetic suppression of component magnetic reconnection at the magnetopause, *J. Geophys. Res.*, *108*(A5), 1218, doi:10.1029/2002JA009726.

[22] Swisdak, M., M. Opher, J. F. Drake, and F. Alouani Bibi (2010), The vector direction of the interstellar magnetic field outside the heliosphere, *Ap. J.*, *710*(2), 1769–1775, doi:10.1088/0004-637X/710/2/1769.

[23] Zeiler, A., D. Biskamp, J. F. Drake, B. N. Rogers, M. A. Shay, and M. Scholer (2002), Three-dimensional particle simulations of collisionless magnetic reconnection, *J. Geophys. Res.*, *107*(A9), 1230, doi: 10.1029/2001JA000287.